Supplementary information for

Unprecedented recent summer warming and cross-sphere hydrological coupling in Asian Water Towers

Youping Chen [1, 2, 4], Feng Chen [1, 2, 3*], Mao Hu [1, 3], Xiaoen Zhao [1, 3], Honghua Cao [1, 3], Shijie Wang[1, 2], Jan Esper [5, 6], Ulf Büntgen [6, 7, 8], Max C. A. Torbenson [5], Tiyuan Hou [1, 2], Hongfan Xu [1, 3], Yufeng Lin [1]

1 Yunnan Key Laboratory of International Rivers and Transboundary Eco-Security/Ministry of Education Key Laboratory for Transboundary Eco-Security of Southwest China, Institute of International Rivers and Eco-Security, Yunnan University, Kunming, China

2 State Key Laboratory of Vegetation Structure, Functions and Construction (VegLab), Yunnan University, Kunming, China

3 Southwest United Graduate School, Kunming, China

4 School of Ecology and Environmental Science, Yunnan University, Kunming, China

5 Department of Geography, Johannes Gutenberg University, Mainz, Germany

6 Global Change Research Institute (CzechGlobe), Czech Academy of Sciences, Brno, Czech Republic.

7 Department of Geography, University of Cambridge, Cambridge, United Kingdom.

8 Department of Geography, Faculty of Science, Masaryk University, Brno, Czech Republic.

*Corresponding Author: feng653@163.com (Feng Chen)

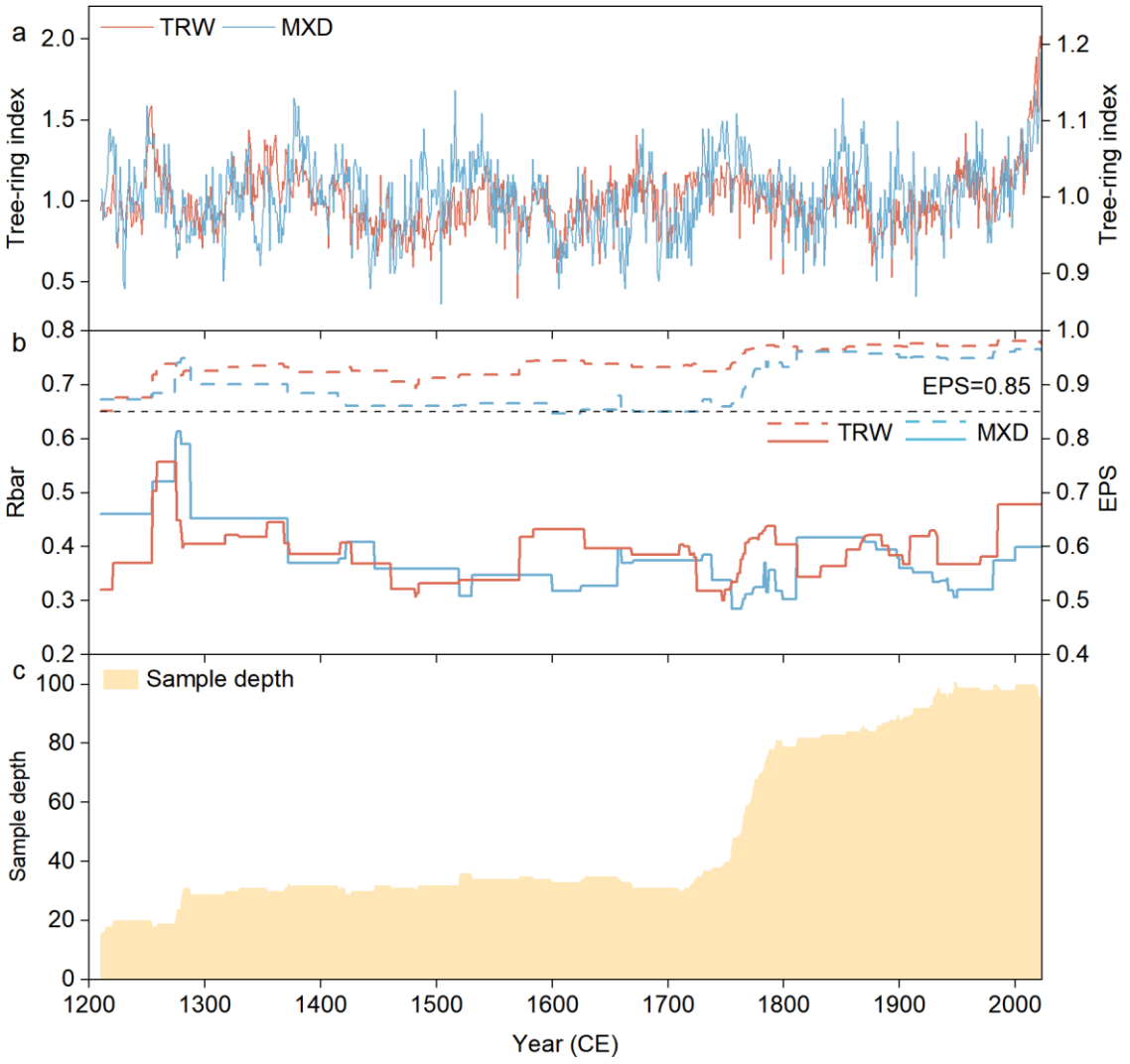

Supplementary Figure 1 Tree-ring width chronologies (TRW) and maximum late density chronologies (MXD). Comparison of tree-ring width chronologies and density chronologies (a), including the Expressed Population Signal (EPS) and the Mean Interseries Correlation (Rbar) (b), as well as the sample depth for both width and density chronologies (c).

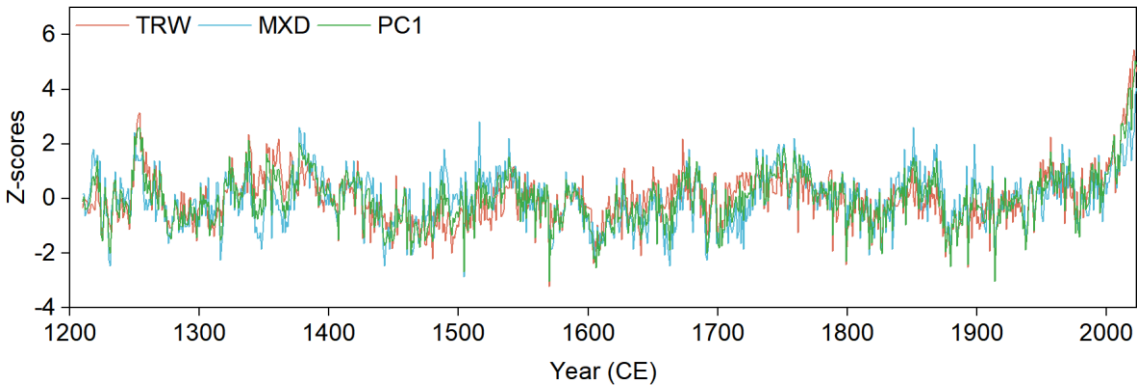

Supplementary Figure 2 Comparison of TRW and MXD normalized sequences with the first principal component sequence (PC1).

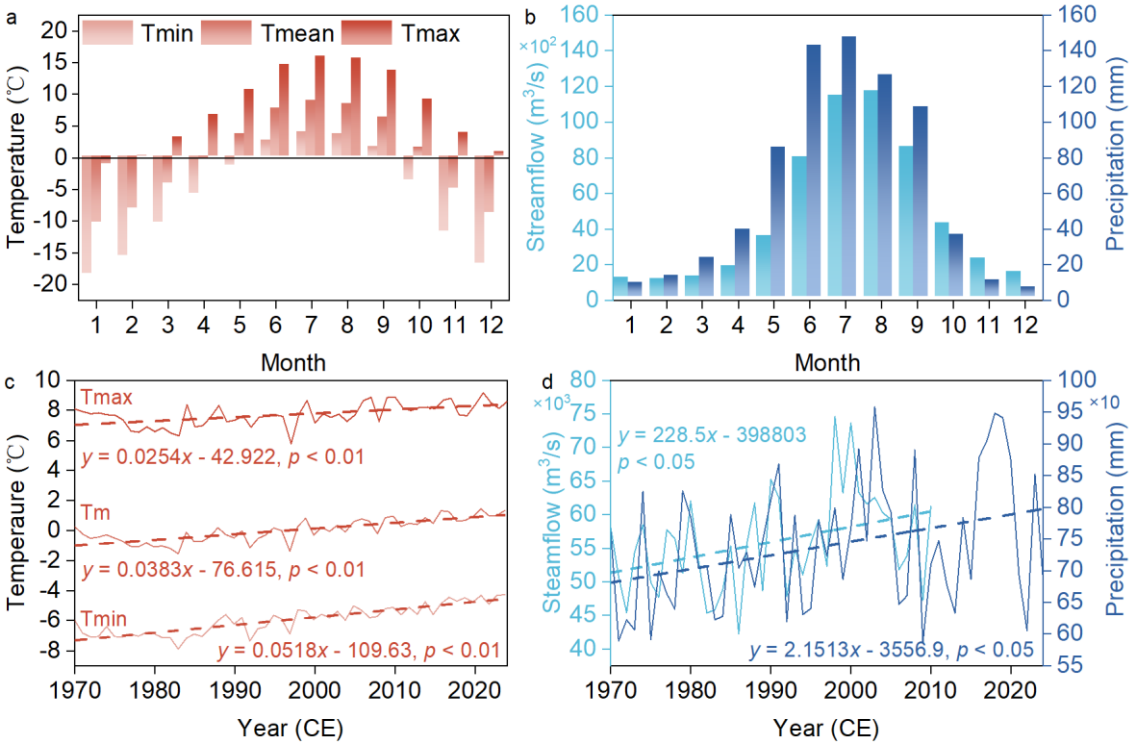

Supplementary Figure 3 Characteristics of climatic and hydrological changes. (a) Intra-annual variation characteristics of the average minimum temperature (Tmin), average temperature (Tm), and average maximum temperature (Tmax) at Jiali Meteorological Station during 1970–2024. (b) Intra-annual variation characteristics of the total precipitation at the Jiali Meteorological Station and the total streamflow at the Kachura, Nuxia, and Daojieba Hydrological Stations during 1970–2010. (c) is the same as (a), and (d) is the same as (b), but they represent the inter-annual variation characteristics.

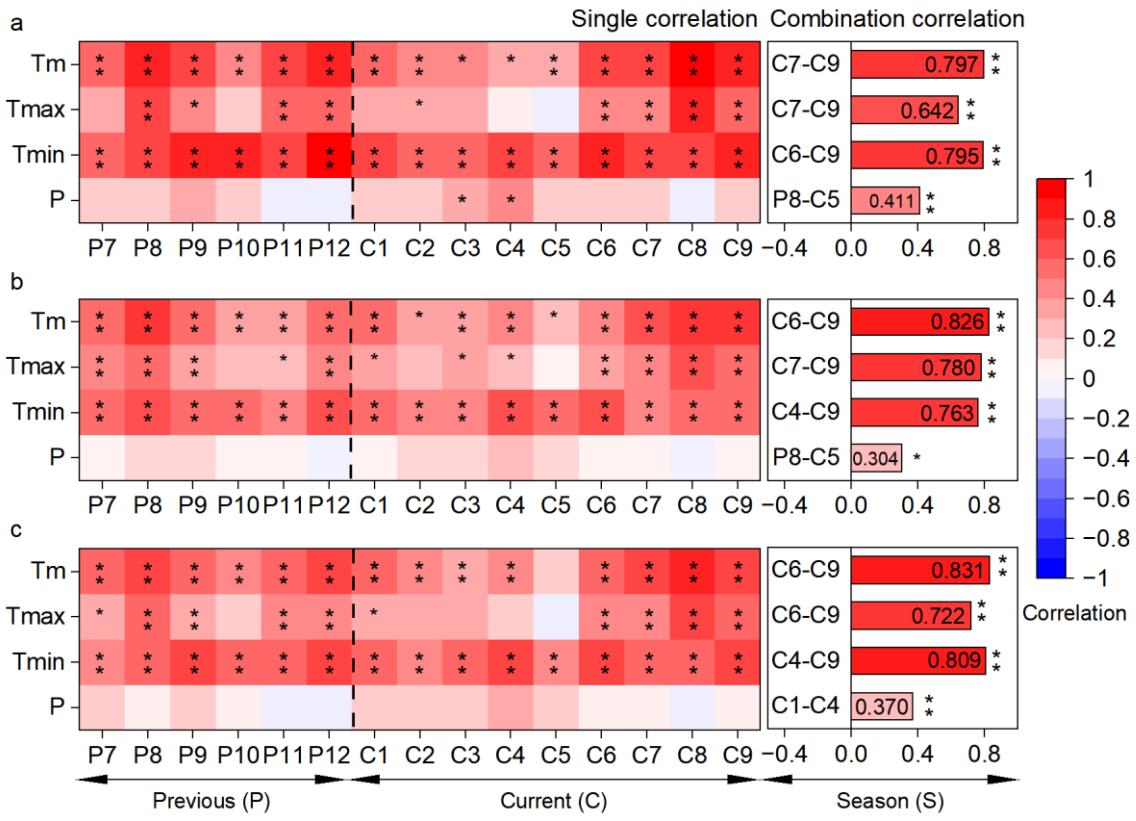

Supplementary Figure 4 Correlations between the TRW (a) MXD (b) and PC1 (c) and monthly meteorological data. The left figure shows monthly single correlation analysis results from July of the previous year (P) to September of the current year (C). The right figure shows the highest correlation coefficient for different month combinations, where Tm is the mean temperature, Tmax is the mean maximum temperature, Tmin is mean minimum temperature, P is total precipitation. * indicates the 95% confidence level, ** indicates the 99% confidence level.

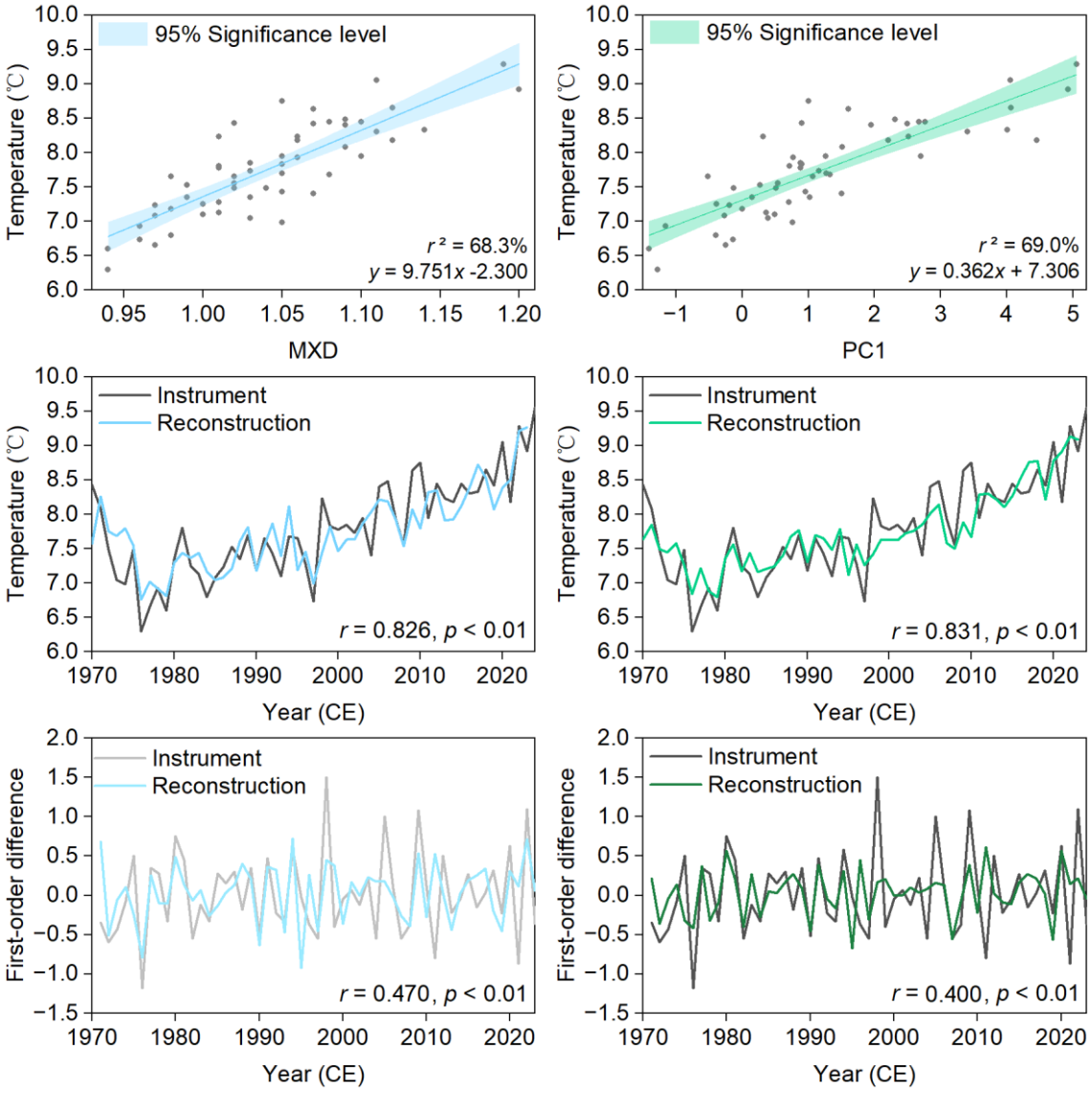

Supplementary Figure 5 Relationships between reconstructed and observed summer temperatures during the common period 1970–2023. Scatter plots and linear regressions between MXD, PC1, and the instrumental mean June–September temperature (a, b). Comparison of the original reconstructed and observed temperature series (c, d). Same as (c, d) but for first-order differences (e, f).

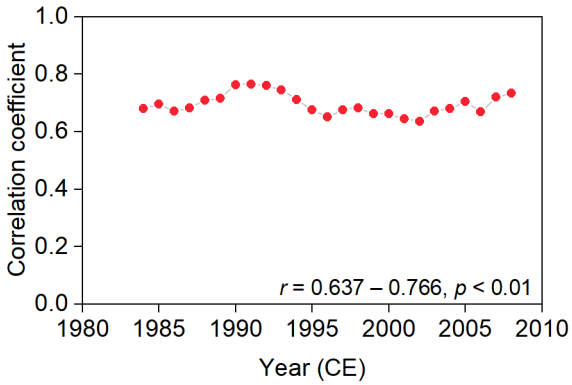

Supplementary Figure 6 The 30-year sliding correlation between the instrumental average temperature series and the reconstructed average temperature series for the period June–September from 1970 to 2023.

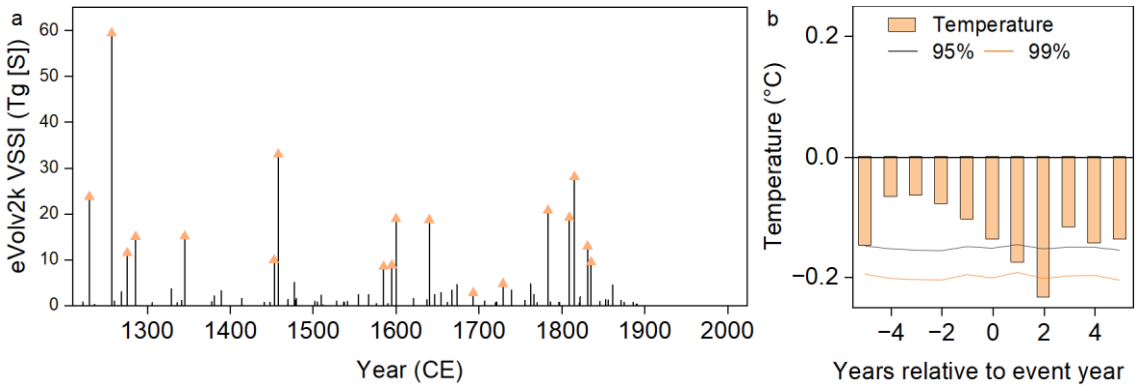

Supplementary Figure 7 (a) Reconstructed volcanic stratospheric sulfur injection (VSSI) from 1200 to 1900 CE, based on the eVolv2k database, with high-magnitude events for superposed epoch analysis marked (yellow triangles). (b) Superposed epoch analysis of these selected events.

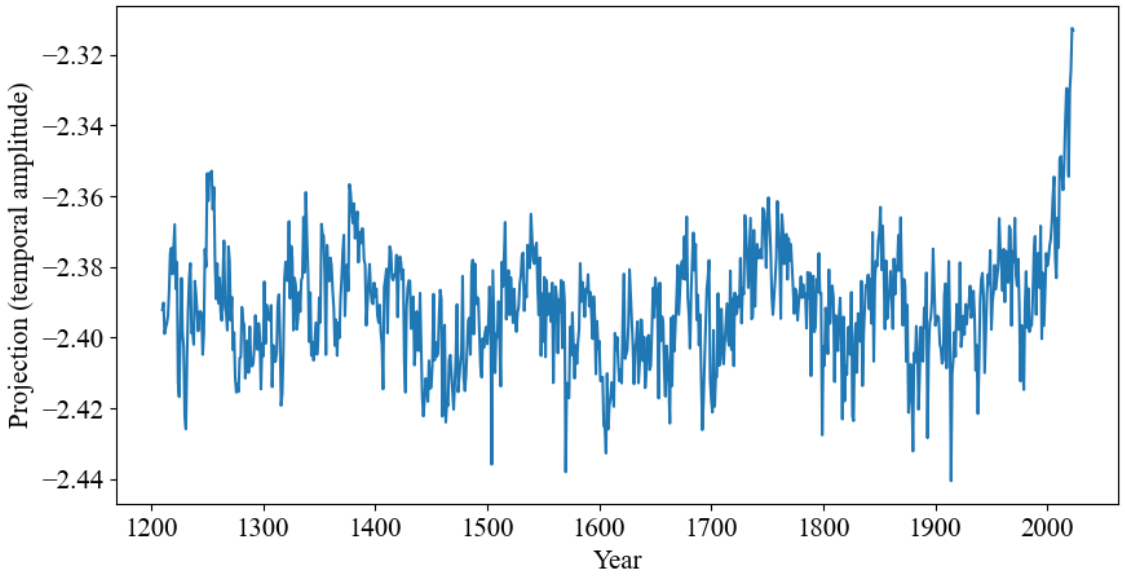

Supplementary Figure 8 Projection of our reconstruction onto the time series derived from the model fingerprint (see Exploration of temperature drivers)

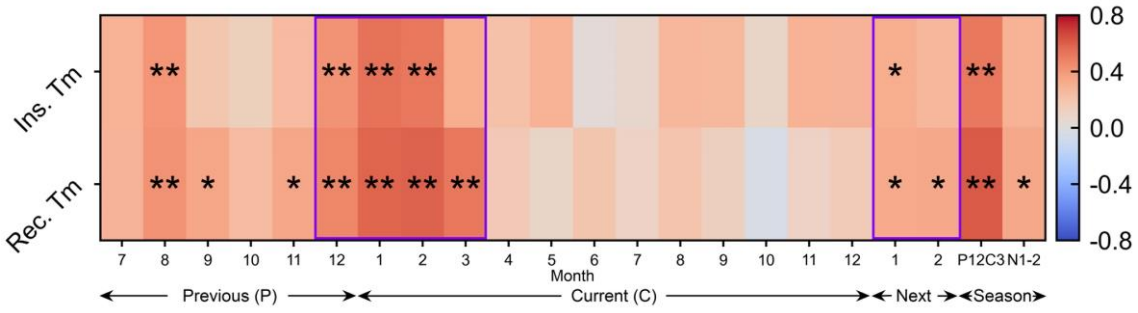

Supplementary Figure 9 Correlation analysis results between the instrumental and reconstructed series of mean air temperature from June to September and the monthly total discharge at the Kachura, Nuxia, and Daojieba hydrological stations during 1970–2010. The purple boxes highlight their close correlation in winter.

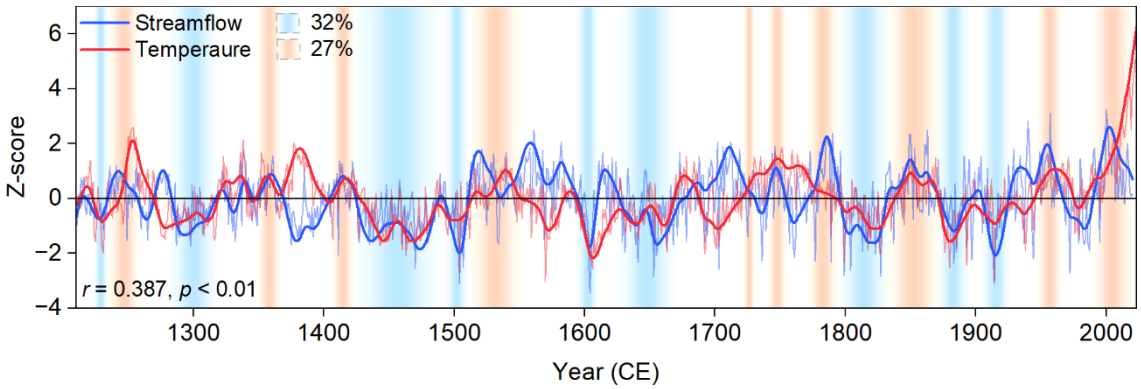

Supplementary Figure 10 Comparison of the reconstructed June–September temperature series from this study (thin line) with the reconstructed total streamflow of the Mekong, Salween, and Yarlung Zangbo Rivers from the previous September through the current July. Both the raw values (thin lines) and their 21-year low-pass filtered trends (thick lines) are shown. The blue and orange backgrounds represent the coordinated weakening and strengthening of the two series.

Supplementary Table 1 Information about the sampling site, meteorological station, and hydrological stations.

Code	Lat. (N)	Lon. (E)	Elevation (m)	Period	Cores/ trees	Tree species
JLC	30.67	94.46	3951.8	1210-2023	31/79	*Picea likiangensis*
Jiali	30.67	93.28	4488.8	1970-2024		
Kachura	35.45	75.42	2341	1970-2010		
Nuxia	20.27	100.08	2910	1970-2010		
Daojieba	24.98	98.88	685	1970-2010		

Supplementary Table 2 Leave-one-out and split-sample validation statistics for the temperature reconstruction.

	Calibration (1970–1995)	Verification (1996–2023)	Calibration (1996–2023)	Verification (1970–1995)	Total (1970-2023)
r	0.719**	0.725**	0.725**	0.719**	0.816**
r^2	0.516	0.525	0.525	0.516	0.666
RE		0.376		0.454	0.666
PMT		4.298		4.530	6.033
ST		$23^{+}/5^{-}$**		$19^{+}/7^{-}$**	$43^{+}/11^{-}$**

Note: RE, PMT, ST, *, and ** represent the reduction of error, product mean test, sign test, 95% confidence level, and 99% confidence level, respectively.

Supplementary Table 3 Year and latitude/longitude information for strong eruptions with VEI ratings ≥ 5 since 1210 CE.

Year	Name	VEI	Lat	Lon
1257	Samalas	7	0.85°S	78.9°W
1480	St. Helens	5	46.2°N	122.18°W
1580	Billy Mitchell	6	6.102°S	105.423°E
1600	Huaynaputina	6	8.25°S	118°E
1640	Parker	5	6.113°N	124.892°E
1652	Sheveluch	5	56.653°N	161.36
1660	Long Island	6	8.42°S	116.47°E
1663	Toya	5	42.544°N	140.839°E
1707	Fujisan	5	35.361°N	138.728°E
1815	Tambora	7	5.358°S	147.12°E
1835	Cosiguina	5	12.98°N	87.57°W
1883	Krakatau	6	6.092°S	155.225°E
1886	Okataina	5	-38.12°S	176.5°E
1902	Santa Maria	6	16.608°S	0.85°W
1912	Novarupta	6	58.27°N	155.157°W
1991	Pinatuba	6	15.13°N	120.35°E

Supplementary Table 4 The CMIP6 models used in this study.

Model	Source	Number (Lat × Lon)	Model	Source	Number (Lat × Lon)
ACCESS-CM2	Australia	144×192	FGOALS-g3	China	80×180
ACCESS-ESM1-5	Australia	145×192	GFDL-ESM4	America	180×288
BCC-CSM2-MR	China	160×320	INM-CM4-8	Russia	120×180
CanESM5	Canada	64×128	INM-CM5-0	Russia	120×180
CAS-ESM2-0	China	128×256	IPSL-CM6A-LR	Europe	143×144
CMCC-CM2-SR5	Italy	192×288	KACE-1-0-G	Korea	80×96
CMCC-ESM2	Italy	192×288	MIROC6	Japan	128×256
EC-Earth3-Veg	Europe	256×512	MPI-ESM1-2-HR	German	192×384
EC-Earth3-Veg-LR	Europe	160×320	MPI-ESM1-2-LR	German	96×192
FGOALS-f3-L	China	192×288	MRI-ESM2-0	Japan	160×320

Supplementary Table 5 Statistical parameters for path estimation and uncertainty in structural equation models

Pathway	β	95 % UL	95 % LL	*p*	RC
Q → NDVI	0.58	0.196	0.804	< 0.01	0.000
NDVI → Albedo	-0.38	-0.652	0.020	0.032	0.000
Albedo → Tm	-0.51	-0.736	-0.254	< 0.01	-0.178
Q → SM	0.38	0.010	0.663	0.029	0.000
SM → LHF	0.864	0.640	0.955	< 0.01	0.000
SM → NDVI	-0.59	-0.790	-0.357	< 0.01	0.000
LHF → Tm	0.31	0.055	0.547	0.034	0.039
Q → Tm	0.32	-0.001	0.636	0.031	0.416

Note: Pathway variables include instrumental runoff (Q), mean temperature (Tm), Normalized Difference Vegetation Index (NDVI), soil moisture (SM), surface albedo, and latent heat flux (LHF). β indicates the standardized regression coefficient, 95% UL and 95% LL denote the 95% confidence upper and lower limits, respectively. *p* indicates the probability value, and RC represents residual covariances.